

Periodically forced delay limit cycle oscillator



Lauren Lazarus, Matthew Davidow, Richard Rand*

Cornell University, Ithaca, NY, USA

ARTICLE INFO

Article history:

Received 7 June 2016

Accepted 4 July 2016

Available online 7 July 2016

Keywords:

Differential-delay equation

Limit cycle oscillator

Entrainment

Non-linear dynamics

ABSTRACT

This paper investigates the dynamics of a delay limit cycle oscillator under periodic external forcing. The system exhibits quasiperiodic motion outside of a resonance region where it has periodic motion at the frequency of the forcer for strong enough forcing. By perturbation methods and bifurcation theory, we show that this resonance region is asymmetric in the frequency detuning, and that there are regions where stable periodic and quasiperiodic motions coexist.

© 2016 Elsevier Ltd. All rights reserved.

1. Introduction

The following equation is perhaps the simplest possible differential-delay equation (DDE) that has interesting dynamics [1,2]:

$$\frac{dx}{dt}(t) = -x(t-T) - x^3(t) \quad (1)$$

It combines delay with nonlinearity and exhibits a Hopf bifurcation. Although it involves only a first derivative in time, it is, as a DDE, infinite dimensional. Thus unlike first order ODEs, which are dynamically much simpler than second order ODEs (for example autonomous first order ODEs cannot oscillate), Eq. (1) supports a limit cycle oscillation.

In this work we shall refer to Eq. (1) as a delay limit cycle oscillator (DLCO). Variants of Eq. (1) have been the subject of two recent studies. These have involved Eq. (1) under linear self-feedback [3], i.e.

$$\frac{dx}{dt}(t) = -x(t-T) - x^3(t) + \alpha x(t) \quad (2)$$

and under a periodic variation within the delay term [4], i.e.

$$\frac{dx}{dt}(t) = -x(t-T) - \epsilon x^3(t), \quad T = \frac{\pi}{2} + \epsilon k + \epsilon \cos \omega t \quad (3)$$

In the present work we continue our investigation of variants of the DLCO by studying the effect of a periodic forcing term:

$$\frac{dx}{dt}(t) = -x(t-T) - \epsilon x^3(t) + \epsilon \alpha \cos \omega t \quad (4)$$

The linearized version of Eq. (1),

$$\frac{dx}{dt}(t) = -x(t-T) \quad (5)$$

has been applied to the growth of sunflowers relative to the angle of the sun [5], and to the motion of beetles in tracking their prey [6].

2. Derivation of slow flow

Since Eq. (1) exhibits a Hopf at $T = \pi/2$, we perturb off of that critical value:

$$T = \frac{\pi}{2} + \epsilon \quad (6)$$

We define two time variables:

$$\xi = \omega t, \quad \eta = \epsilon t, \quad \text{where } \omega = 1 + \epsilon \Delta \quad (7)$$

Then the first derivative is expanded into two terms:

$$\frac{dx}{dt} = \frac{\partial x}{\partial \xi} \frac{d\xi}{dt} + \frac{\partial x}{\partial \eta} \frac{d\eta}{dt} = \frac{\partial x}{\partial \xi} (1 + \epsilon \Delta) + \frac{\partial x}{\partial \eta} \epsilon \quad (8)$$

Additionally, the delayed term is expanded as a Taylor series for small ϵ :

$$x(t-T) = x(\xi - \omega T, \eta - \epsilon T) \quad (9)$$

$$x(t-T) = x(\xi - (1 + \epsilon \Delta)T, \eta - \epsilon T) \quad (10)$$

* Corresponding author.

E-mail address: rhr2@cornell.edu (R. Rand).

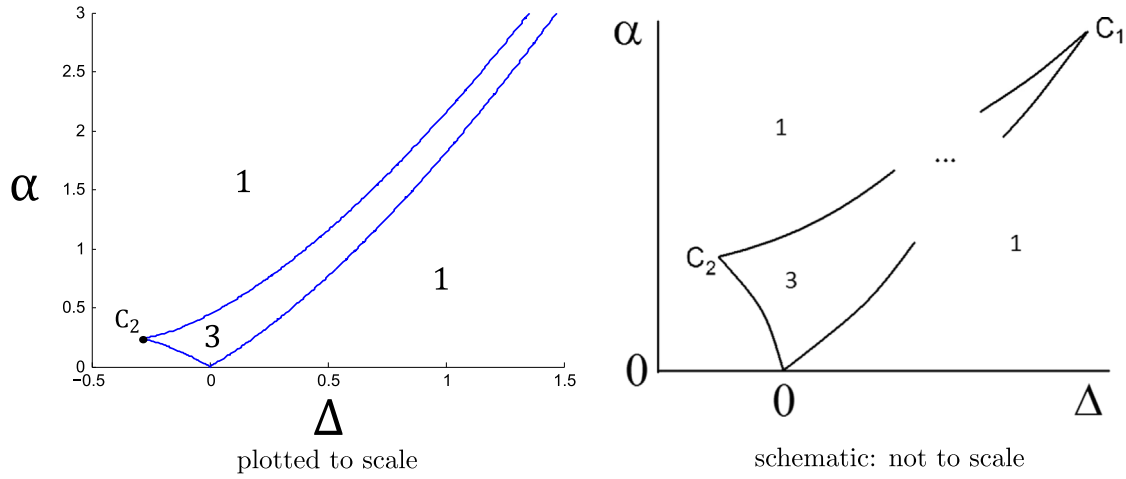


Fig. 1. Saddle-node bifurcation curves (Eq. (27)) in (Δ, α) parameter space for $\alpha \geq 0$. The number of equilibrium points in each region is also labeled. The curves meet in two cusps, C_1, C_2 , as well as at the origin.

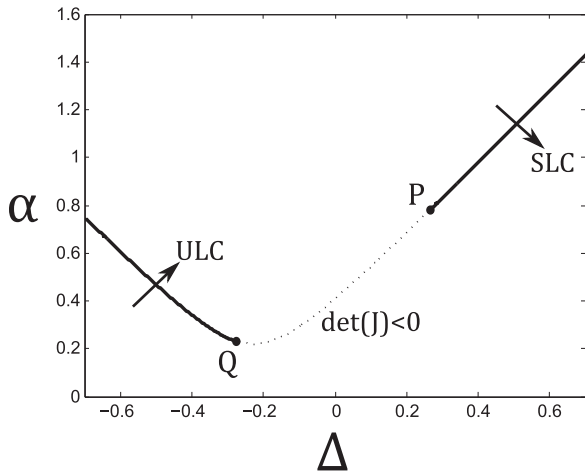


Fig. 2. Hopf bifurcation curve given as two branches of the $\text{tr}(J) = 0$ condition (Eq. (33)), resulting in a stable limit cycle (SLC) or unstable limit cycle (ULC). When $\det(J) < 0$ (between points P and Q), the $\text{tr}(J) = 0$ curve is not a Hopf bifurcation.

$$x(t - T) = x\left(\xi - (1 + \epsilon\Delta)\left(\frac{\pi}{2} + \epsilon\right), \eta - \epsilon\frac{\pi}{2}\right) + O(\epsilon^2) \tag{11}$$

$$x(t - T) = x\left(\xi - \frac{\pi}{2} - \epsilon\left(\Delta\frac{\pi}{2} + 1\right), \eta - \epsilon\frac{\pi}{2}\right) + O(\epsilon^2) \tag{12}$$

$$x(t - T) = \bar{x} - \epsilon\left[\left(\Delta\frac{\pi}{2} + 1\right)\frac{\partial\bar{x}}{\partial\xi} + \frac{\pi}{2}\frac{\partial\bar{x}}{\partial\eta}\right] + O(\epsilon^2) \tag{13}$$

where $\bar{x} = x\left(\xi - \frac{\pi}{2}, \eta\right)$.

Next we expand

$$x = x_0 + \epsilon x_1 + O(\epsilon^2) \tag{14}$$

and substitute Eq. (14) into Eq. (4), collect terms and set coefficients of like powers of ϵ equal to zero. This gives:

$$Lx_0 = 0 \tag{15}$$

$$Lx_1 = -\frac{\partial x_0}{\partial \xi}\Delta - \frac{\partial x_0}{\partial \eta} + \left(\Delta\frac{\pi}{2} + 1\right)\frac{\partial \bar{x}_0}{\partial \xi} + \frac{\pi}{2}\frac{\partial \bar{x}_0}{\partial \eta} - x_0^3 + \alpha \cos \xi \tag{16}$$

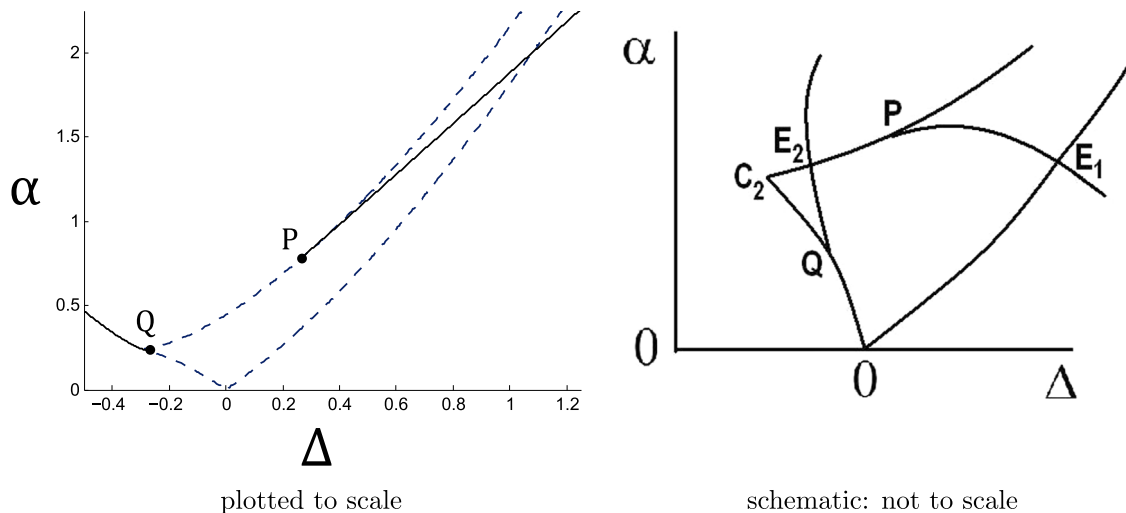


Fig. 3. Saddle-node (Eq. (27)) and Hopf bifurcation (Eq. (33)) curves plotted in (Δ, α) parameter space for $\alpha \geq 0$. These results have also been confirmed with AUTO bifurcation continuation software [8].

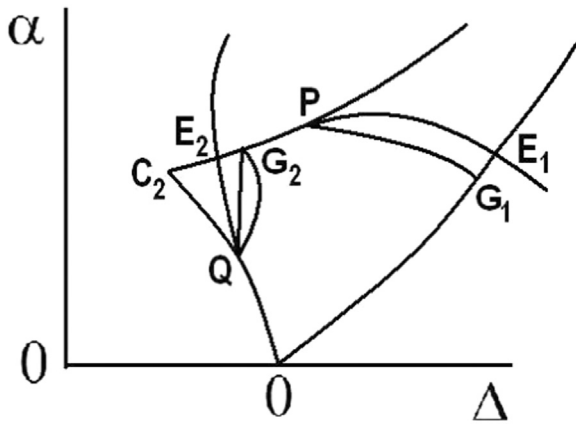


Fig. 4. Homoclinic bifurcations $P - G_1$ and $Q - G_2$ are shown along with Hopf bifurcations $P - E_1$ and $Q - E_2$. Cf. Fig. 3. This figure is schematic and is not drawn to scale.

where

$$Lx_i = \frac{\partial x_i}{\partial \xi} + \tilde{x}_i \tag{17}$$

Note that Eq. (16) can be simplified by using Eqs. (15), (17) to write

$$\frac{\partial \tilde{x}_0}{\partial \xi} = -\frac{\partial^2 x_0}{\partial \xi^2}, \quad \frac{\partial \tilde{x}_0}{\partial \eta} = -\frac{\partial^2 x_0}{\partial \eta \partial \xi} \tag{18}$$

giving

$$Lx_1 = -\frac{\partial x_0}{\partial \xi} \Delta - \frac{\partial x_0}{\partial \eta} - \left(\Delta \frac{\pi}{2} + 1 \right) \frac{\partial^2 x_0}{\partial \xi^2} - \frac{\pi}{2} \frac{\partial^2 x_0}{\partial \eta \partial \xi} - x_0^3 + \alpha \cos \xi \tag{19}$$

Eq. (15), representing the unperturbed equation, has the general solution:

$$x_0 = A(\eta) \cos \xi + B(\eta) \sin \xi \tag{20}$$

Substituting Eq. (20) into Eq. (19) and removing secular terms

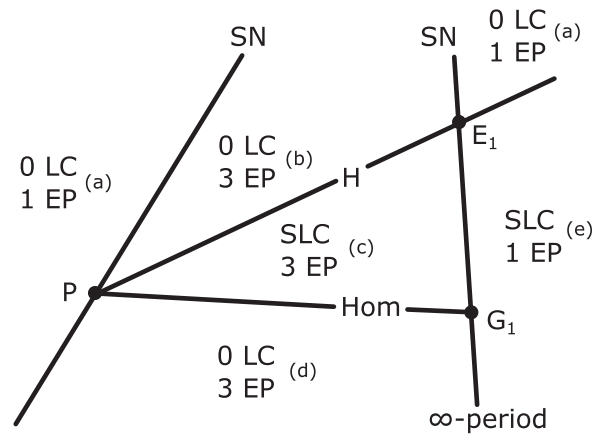


Fig. 6. Schematic of bifurcation curves around points P , E_1 , and G_1 : saddle-node (SN), Hopf (H), and homoclinic (Hom). The limit cycles (LC) and number of equilibrium points (EP) are also shown for each region. The right SN becomes an infinite-period bifurcation below point G_1 . Labels (a–e) correspond to Fig. 7, where representative phase portraits are given.

gives the following slow flow:

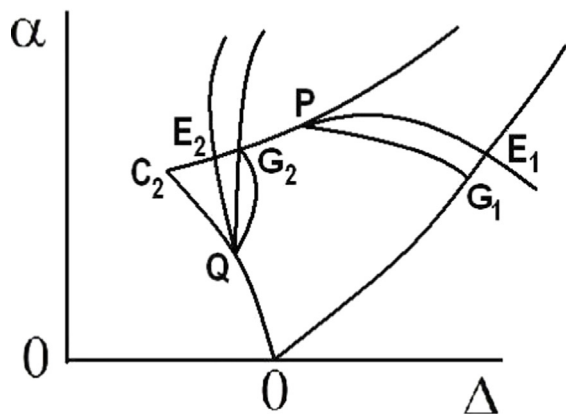
$$\frac{dA}{d\eta} = -\frac{(2\pi^2 + 8)B\Delta - 3\pi B^3 + 6AB^2 + (4\pi - 3\pi A^2)B - 8\alpha + 6A^3 - 8A}{2\pi^2 + 8} \tag{21}$$

$$\frac{dB}{d\eta} = \frac{(2\pi^2 + 8)A\Delta - 6B^3 - 3\pi AB^2 + (8 - 6A^2)B + 4\pi\alpha - 3\pi A^3 + 4\pi A}{2\pi^2 + 8} \tag{22}$$

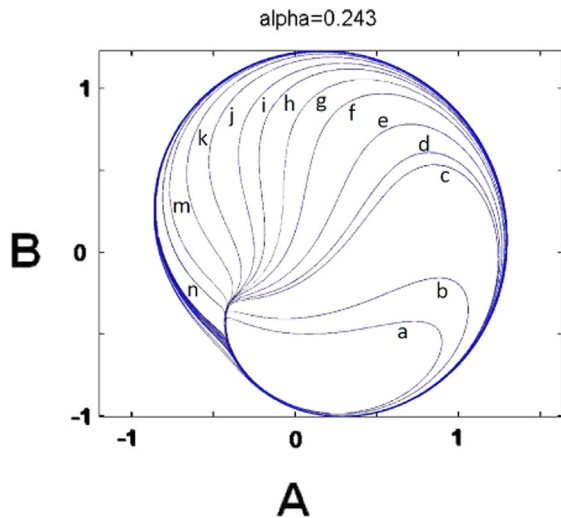
3. Analysis of slow flow

3.1. Equilibria and saddle-node bifurcations

We begin by looking for the equilibrium points of the slow flow, which satisfy:



schematic: not to scale



plotted to scale

Fig. 5. Limit cycle fold bifurcations occur along a curve which starts at point G_2 and extends upwards in the direction of increasing α . The figure on the right shows a sequence of slow flow phase plane plots for fixed $\alpha = 0.243$ and increasing Δ for trajectories marked (a–n). Curve a corresponds to $\Delta = -0.2850$ and curve n corresponds to $\Delta = -0.282691$.

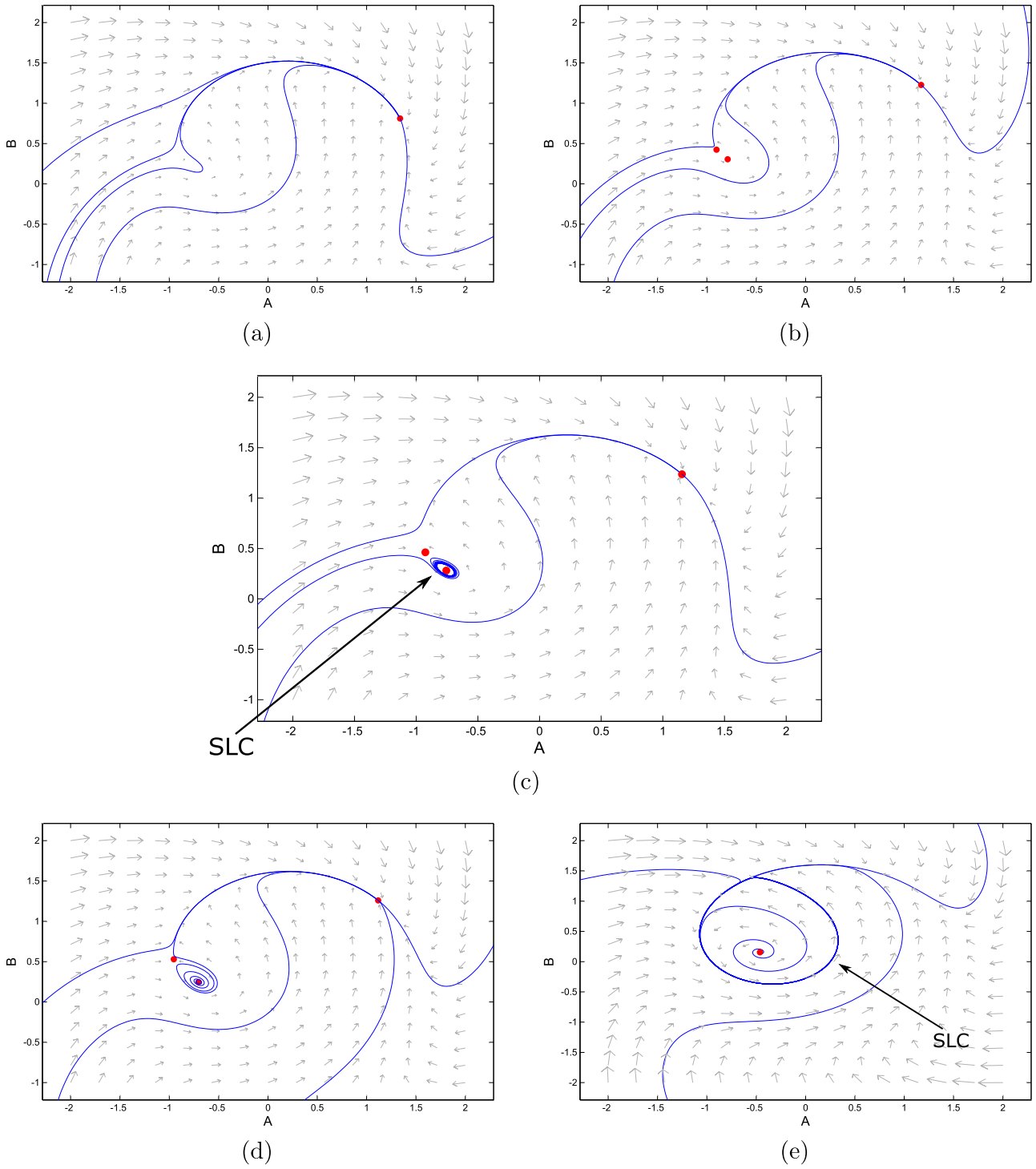


Fig. 7. Representative phase portraits in (A, B) from each region (a–e) of parameter space from Fig. 6. A stable limit cycle exists only in regions (c) and (e), as marked. Obtained with numerical integration via `pplane` [7].

$$0 = -(2\pi^2 + 8)B\Delta + 3\pi B^3 - 6AB^2 - (4\pi - 3\pi A^2)B + 8\alpha - 6A^3 + 8A \tag{23}$$

$$0 = (2\pi^2 + 8)A\Delta - 6B^3 - 3\pi AB^2 + (8 - 6A^2)B + 4\pi\alpha - 3\pi A^3 + 4\pi A \tag{24}$$

First note that $A = B = 0$ (corresponding to $x(t) = 0$) is not an equilibrium solution, due to the presence of the forcing term α . Using Maxima to eliminate B from this set of equations gives a

cubic equation $f(A) = 0$:

$$f(A) = 9\alpha^2 A^3 + 24\alpha\Delta^2 A^2 + 16\Delta^2 A + 16\pi\Delta^3 A - 12\alpha^2 A + 4\pi^2\Delta^4 A + 16\Delta^4 A - 6\pi\alpha^2\Delta A + 16\alpha\Delta^2 + 8\pi\alpha\Delta^3 - 12\alpha^3 = 0 \tag{25}$$

To search for double roots, which will signify saddle-node bifurcations, we look for the condition $f'(A) = 0$ to be satisfied simultaneously with $f(A) = 0$:

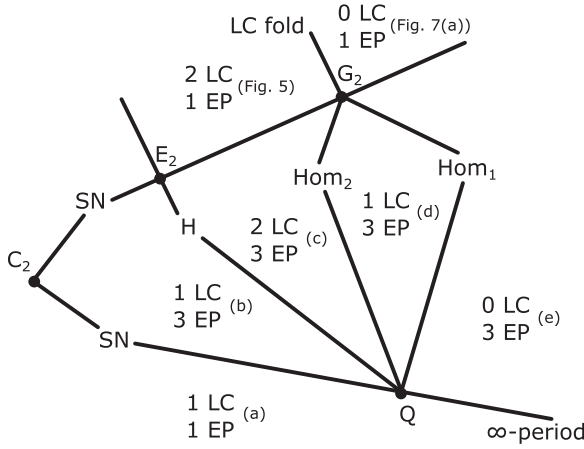


Fig. 8. Schematic of bifurcation curves around points Q , E_2 , and G_2 : saddle-node (SN), Hopf (H), homoclinic (Hom), and limit cycle fold (LC fold). The limit cycles (LC) and number of equilibrium points (EP) are also shown for each region. Labels (a–e) correspond to Fig. 9, where representative phase portraits are given.

$$f'(A) = 27\alpha^2 A^2 + 48\alpha\Delta^2 A + 16\Delta^2 + 16\pi\Delta^3 - 12\alpha^2 + 4\pi^2\Delta^4 + 16\Delta^4 - 6\pi\alpha^2\Delta = 0 \quad (26)$$

By eliminating A from this pair of Eqs. (25), (26), we find multiple expressions where the equilibrium value of A occurs at a double root. By considering the same process to find double roots in B , eliminating A from the equations first, we eliminate extraneous results. The remaining saddle-node bifurcation curve is found at:

$$4\pi^4\Delta^6 + 32\pi^2\Delta^6 + 64\Delta^6 + 32\pi^3\Delta^5 + 128\pi\Delta^5 + 96\pi^2\Delta^4 + 128\Delta^4 - 6\pi^3\alpha^2\Delta^3 - 216\pi\alpha^2\Delta^3 + 128\pi\Delta^3 - 36\pi^2\alpha^2\Delta^2 - 432\alpha^2\Delta^2 + 64\Delta^2 - 72\pi\alpha^2\Delta + 243\alpha^4 - 48\alpha^2 = 0 \quad (27)$$

Note that α only appears at even powers; the transformation $\alpha \rightarrow -\alpha$ only affects the phase of the forcing term, which has no effect due to the autonomous nature of the system. We will take $\alpha \geq 0$ for simplicity.

Fig. 1 shows the saddle-node bifurcation curves and marks the regions of 1 and 3 equilibrium points.

The saddle-node bifurcation curves meet in cusps where the equilibrium is a triple root of the system. To find the locations of the cusps, we look for triple roots in A by finding $f''(A) = 0$:

$$f''(A) = 54\alpha^2 A + 48\alpha\Delta^2 = 0 \quad (28)$$

Solving this alongside equations (25) and (26), we find the locations of cusps C_1 and C_2 to be:

$$(\Delta, \alpha)_{C_1} = (6.201, 22.126) \quad (29)$$

$$(\Delta, \alpha)_{C_2} = (-0.3027, 0.2386) \quad (30)$$

These cusps may also be seen in Fig. 1.

3.2. Hopf bifurcations

Consider the equilibrium points to be (A_E, B_E) . Then linearize the slow flow about the equilibrium point and construct the Jacobian matrix J :

$$(2\pi^2 + 8)J = \begin{bmatrix} 18A_E^2 - 6\pi A_E B_E + 6B_E^2 - 8 & 4\pi + (2\pi^2 + 8)\Delta - 3\pi A_E^2 + 12A_E B_E - 9\pi B_E^2 \\ -4\pi - (2\pi^2 + 8)\Delta + 9\pi A_E^2 + 12A_E B_E + 3\pi B_E^2 & 6A_E^2 + 6\pi A_E B_E + 18B_E^2 - 8 \end{bmatrix} \quad (31)$$

For a Hopf bifurcation, we require $\text{tr}(J) = 0$ and $\det(J) > 0$. The first condition takes the form:

$$3(A_E^2 + B_E^2) - 2 = 0 \quad (32)$$

We solve this alongside the equilibrium conditions in A_E and B_E to acquire several equations in Δ and α . Extraneous expressions are eliminated by numerical observations to give a single equation for Hopf bifurcations:

$$\alpha_H^2 = \frac{1}{6}((\pi^2 + 4)\Delta^2 + 2\pi\Delta + 1) \quad (33)$$

Along this curve, the determinant of the Jacobian changes sign at $\Delta = \pm 1/\sqrt{\pi^2 + 4}$. Eq. (33) represents a Hopf bifurcation provided $\Delta < -1/\sqrt{\pi^2 + 4}$ or $\Delta > 1/\sqrt{\pi^2 + 4}$.

This pair of conditions also corresponds to the intersection of the Hopf bifurcation curve with the saddle-node bifurcation curve, which occurs tangentially at the locations P and Q :

$$(\Delta, \alpha)_P = \left(\frac{1}{\sqrt{\pi^2 + 4}}, 0.7893914 \right) \quad (34)$$

$$(\Delta, \alpha)_Q = \left(-\frac{1}{\sqrt{\pi^2 + 4}}, 0.2283538 \right) \quad (35)$$

The Hopf bifurcation for $\Delta > 1/\sqrt{\pi^2 + 4}$ is observed to be supercritical, creating a stable limit cycle for values of $|\alpha| < \alpha_H$. For $\Delta < -1/\sqrt{\pi^2 + 4}$, the Hopf bifurcation is subcritical, creating an unstable limit cycle for values of $|\alpha| > \alpha_H$. These results are summarized in Fig. 2. These and any other limit cycles in the slow flow (A, B) represent quasiperiodic behavior in the original system $x(t)$.

Fig. 3 shows the saddle-node and Hopf bifurcation curves together. The curves intersect at four locations: P and Q (the tangencies found above), and points labeled E_1 and E_2 . At points E_1 and E_2 , the Hopf bifurcation occurs simultaneously with a saddle-node bifurcation. However, these bifurcations take place at separate equilibrium locations (A_E, B_E) in phase space and do not interact; their simultaneous occurrence in parameter space is a coincidence.

We will explore the behaviors at points P and Q further.

3.3. Homoclinic bifurcations

Numerical integration of the slow flow equations (21), (22) shows that the limit cycles born in the Hopf bifurcations in Fig. 2 are destroyed in homoclinic bifurcations, a common scenario in nonlinear dynamics (see e.g. section 3.3 of [1]). The results of numerical integration are displayed in Fig. 4, where three curves of homoclinic bifurcations are shown. The homoclinic bifurcation along the curve $P - G_1$ absorbs the limit cycle born in the Hopf curve $P - E_1$. Two additional homoclinic bifurcations occur on the curves $Q - G_2$.

3.4. Limit cycle folds

Numerical integration of the slow flow equations (21), (22) reveals another curve of bifurcations, in addition to the saddle-nodes, Hopfs and homoclinics already discussed. A limit cycle fold is found for $\Delta < 0$ where a pair of limit cycles (stable and unstable)

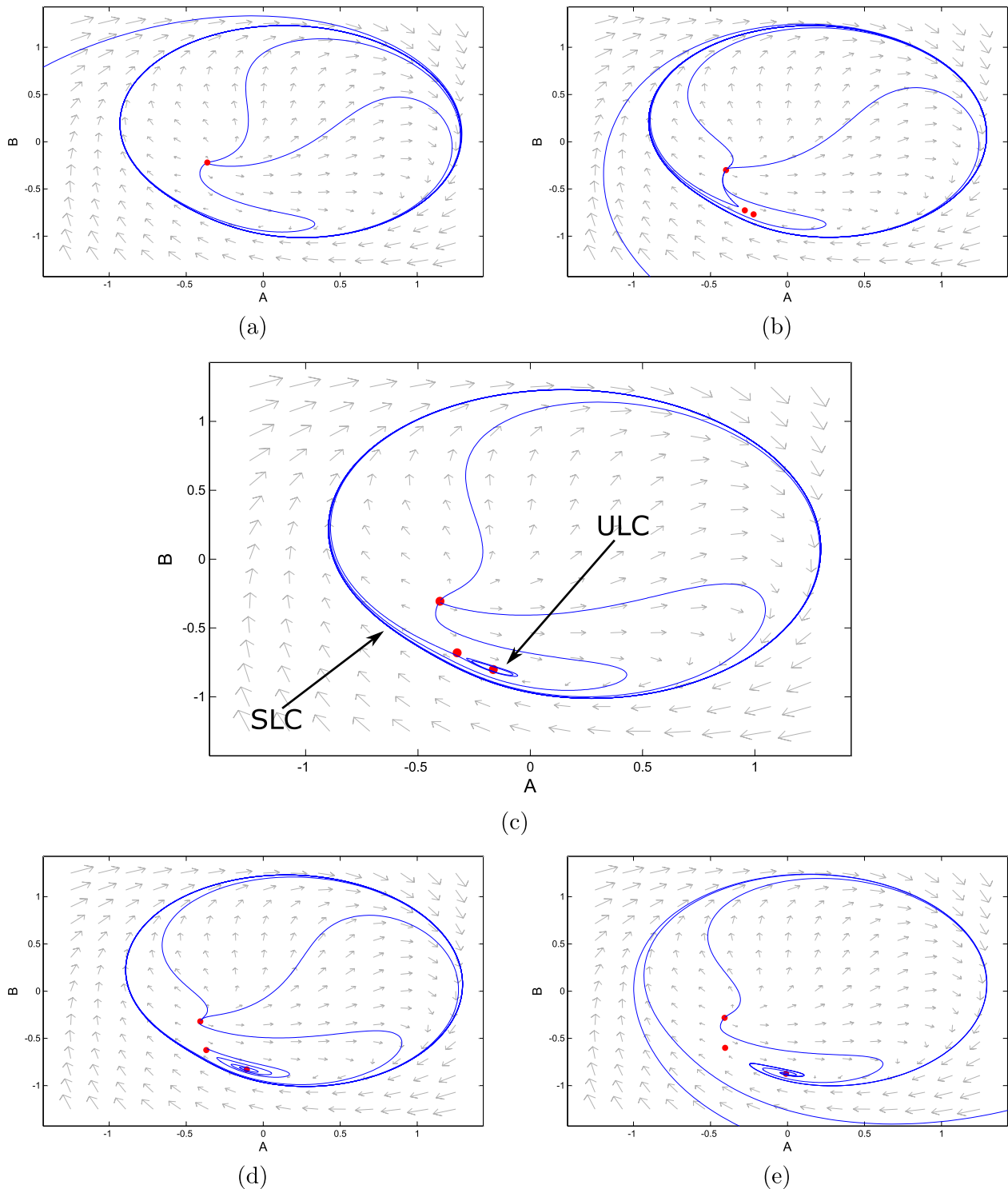


Fig. 9. Representative phase portraits in (A, B) from each region (a–e) of parameter space from Fig. 8. A stable limit cycle exists in regions (a–d), while the unstable limit cycle exists only in region (c) as marked. Obtained with numerical integration via `ppplane` [7].

merge and disappear. See Fig. 5, where the limit cycle folds occur along a curve which starts at point G_2 and extends upwards in the direction of increasing α .

The figure on the right side of Fig. 5 shows a sequence of slow flow phase plane plots demonstrating the two limit cycle trajectories, for fixed α and increasing Δ in the neighborhood of the curve of limit cycle folds. The outer stable limit cycle is relatively

unchanged, while the unstable limit cycle, created in the Hopf bifurcation (Eq. (33)), approaches it via trajectories marked (a–n).

The limit cycle fold curve is observed to approach the Hopf bifurcation curve which emanates from point Q , asymptotically as Δ approaches large negative values (away from the resonance region of parameter space). As a result, the region between these curves, which exhibits both a stable limit cycle and a stable

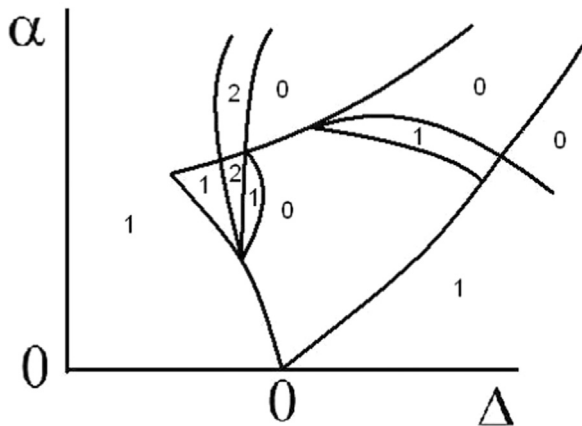


Fig. 10. The number of slow flow limit cycles in each of the regions of Fig. 5 is displayed. There is a stable limit cycle whenever at least one limit cycle exists. This figure is schematic and is not drawn to scale.

equilibrium point, rapidly becomes narrow away from the resonance.

4. Behavior of the slow flow near point P

The Hopf bifurcation branch $P - E_1$ creates a stable limit cycle for smaller values of α , see Fig. 2. This limit cycle is numerically observed to be destroyed in a homoclinic bifurcation along $P - G_1$. The Hopf and homoclinic bifurcations occur at the slow flow equilibrium points which are created in the saddle-node bifurcation near P .

The Hopf and homoclinic bifurcation curves starting at P continue towards the saddle-node bifurcation curve which intersects points E_1 and G_1 . The homoclinic bifurcation curve ends at point G_1 , while the Hopf curve continues through point E_1 into the neighboring region.

The resulting bifurcation diagram near points P , G_1 , and E_1 is shown in Fig. 6. Phase portraits of the slow flow corresponding to the regions labeled (a–d) are displayed in Fig. 7.

5. Behavior of the slow flow near point Q

In Fig. 8 we explore the behavior of the slow flow in the regions around points Q , E_2 , and G_2 . To the left of Fig. 8, away from the resonance, there exists a stable limit cycle L_1 which corresponds to quasiperiodic motion in the original system equation (4). This quasiperiodicity is a result of motions involving both the unforced limit cycle frequency and the forcing frequency.

The region QE_2G_2 contains two limit cycles, one of which is L_1 . The second limit cycle L_2 is a small unstable limit cycle which is created at the Hopf bifurcation branch $Q - E_2$, see Fig. 2. The limit cycle L_2 is numerically observed to be destroyed in a homoclinic bifurcation Hom_2 along $Q - G_2$. Limit cycle L_1 is destroyed in a second homoclinic bifurcation Hom_1 which also intersects points Q and G_2 .

Limit cycle L_1 is destroyed in an infinite-period bifurcation as we cross the saddle-node bifurcation curve to the right of point Q in Fig. 8.

The Hopf and homoclinic bifurcation curves starting at Q continue towards the saddle-node bifurcation curve which intersects points E_2 and G_2 . The Hopf bifurcation curve continues through point E_2 into the neighboring region. The homoclinic curves Hom_1

and Hom_2 , representing the destruction of the limit cycles, meet at point G_2 and are replaced by a limit cycle fold.

Phase portraits of the slow flow corresponding to the regions of Fig. 8 labeled (a–e) are displayed in Fig. 9.

6. Conclusions

In this paper we have studied the effect of applying a periodic forcing function to a delay limit cycle oscillator (DLCO):

$$\frac{dx}{dt}(t) = -x(t-T) - \epsilon x^3(t) + \epsilon \alpha \cos \omega t \quad (36)$$

From Eq. (20) we see that an equilibrium point in the slow flow corresponds to a periodic motion at the same frequency $\omega = 1 + \epsilon \Delta$ as the forcing function. By contrast, a limit cycle in the slow flow corresponds to a quasiperiodic motion in Eq. (36), a motion which may be thought of as having frequencies coming from both the original limit cycle and the forcing function.

Fig. 10 shows the number of slow flow limit cycles in each of the regions of Fig. 5. It may be noted that in regions of at least one limit cycle, a stable limit cycle exists. This indicates that entrainment can only be guaranteed in regions of zero limit cycles (with a stable equilibrium point).

For large enough α , a stable equilibrium point exists in the absence of stable limit cycles, indicating that the forcing function entrains the DLCO when it is strong enough. In contrast, for small α or correspondingly large detuning, the system exhibits a limit cycle as its only stable behavior, indicating that Eq. (36) exhibits quasiperiodic motion.

However, the nature of the transition between quasiperiodic behavior and entrainment does depend on the direction of the detuning Δ , as may be seen in particular from the distinctions between points P and Q . We note that there exist transition regions where multiple stable behaviors coexist, such that entrainment is dependent on the history of the system.

It may also be noted that the behavior for Eq. (36) near the degenerate point P , as shown in Fig. 6, is directly comparable to the forced van der Pol oscillator. (See [9, p. 71], or [1, p. 42b].) This comparison marks a similarity between the behaviors of the DLCO and the forced van der Pol oscillator. No such similarity exists for the behavior near point Q .

References

- [1] R.H. Rand, Lecture Notes in Nonlinear Vibrations published online by the Internet-First University Press: (<http://ecommons.library.cornell.edu/handle/1813/28989>), 2012.
- [2] R. Rand, Differential-delay equations, in: A.C.J. Luo, J.-Q. Sun (Eds.), Complex Systems: Fractionality, Time-delay and Synchronization, Springer, Berlin, 2011, pp. 83–117 (Chapter 3).
- [3] L. Lazarus, M. Davidow, R. Rand, Dynamics of a delay limit cycle oscillator with self-feedback, Nonlinear Dyn. 82 (2015) 481–488.
- [4] L. Lazarus, M. Davidow, R. Rand, Dynamics of an oscillator with delay parametric excitation, Int. J. Non-Linear Mech. 78 (2016) 66–71.
- [5] D. Israelsson, A. Johnsson, A theory for circumnutations in Helianthus annuus, Physiol. Plant. 20 (1967) 957–976.
- [6] A.F. Haselsteiner, C. Gilbert, Z.J. Wang, Tiger beetles pursue prey using a proportional control law with a delay of one half-stride, J. R. Soc. Interface 11 (2014).
- [7] J.C. Polking, pplane is ODE software that runs in MATLAB, see (<http://math.rice.edu/~dfield/index.html>).
- [8] E. Doedel, A. Champneys, T. Fairgrieve, Y. Kuznetsov, B. Sandstede, X. Wang, AUTO 97: Continuation and Bifurcation Software for Ordinary Differential Equations, 1998.
- [9] J. Guckenheimer, P. Holmes, Nonlinear Oscillations, Dynamical Systems, and Bifurcations of Vector Fields, Springer-Verlag, New York, 1983.